IEEE Photonics Journal
An IEEE Photonics Society Publication

Characterization of Plasmonic Modes in a Low-Loss Dielectric-Coated Hollow Core Rectangular Waveguide at Terahertz Frequency

Volume 3, Number 6, December 2011

B. M. A. Rahman, Senior Member, IEEE
Anita Quadir, Student Member, IEEE
Huda Tanvir, Student Member, IEEE
K. T. V. Grattan

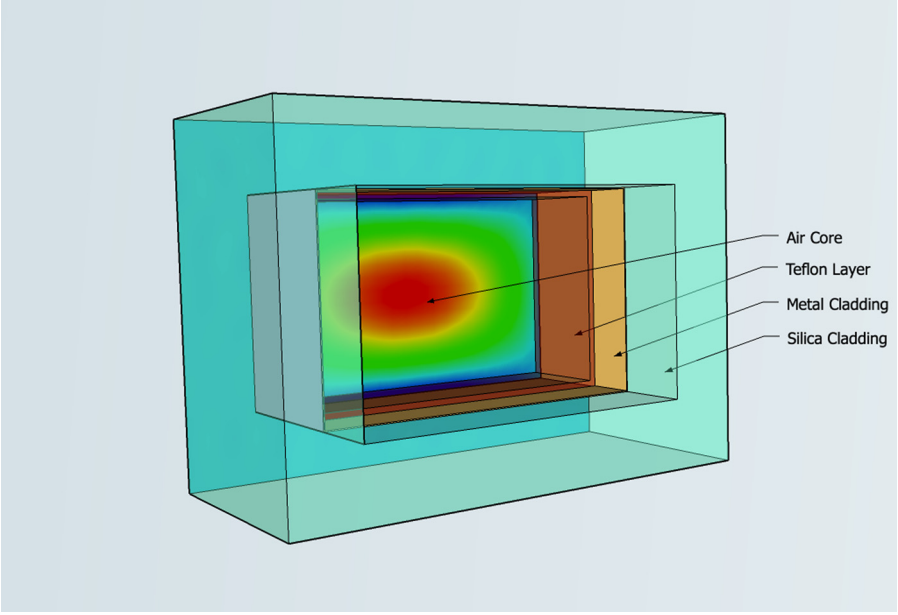

DOI: 10.1109/JPHOT.2011.2173326
1943-0655/$26.00 ©2011 IEEE

IEEE photonics SOCIETY

IEEE

Characterization of Plasmonic Modes in a Low-Loss Dielectric-Coated Hollow Core Rectangular Waveguide at Terahertz Frequency

B. M. A. Rahman, *Senior Member, IEEE*, Anita Quadir, *Student Member, IEEE*, Huda Tanvir, *Student Member, IEEE*, and K. T. V. Grattan

School of Engineering and Mathematical Sciences, City University London, Northampton Square, EC1V 0HB London, U.K.

DOI: 10.1109/JPHOT.2011.2173326
1943-0655/$26.00 ©2011 IEEE

Manuscript received September 1, 2011; revised October 11, 2011; accepted October 16, 2011. Date of publication October 24, 2011; date of current version November 8, 2011. Corresponding author: A. Quadir (e-mail: Anita.Quadir.1@city.ac.uk).

Abstract: In this paper, a low-loss hollow-core rectangular plasmonic waveguide with a dielectric coating of Teflon is analyzed for terahertz (2.5 THz) propagation using a full-vectorial finite-element method (FEM). The modal properties of the waveguide, their effective indices, and power confinements have been calculated with a particular emphasis on the loss characteristics of the different modes. It has been observed that the loss characteristics of the guide are greatly affected by the thickness of the dielectric coating. It has been identified that, in contrast to the fundamental H_{10}^{x} mode, the H_{12}^{x} mode shows interesting modal properties and offers the lowest possible loss for the structure. This mode also tends to yield a near-Gaussian field profile when the dielectric coating thickness is optimized. The optimization of the loss values has been evaluated by comparing the loss characteristics for different dielectric materials, as well as by using different metal claddings.

Index Terms: Finite-element method (FEM), metal-clad dielectric-coated rectangular waveguides, modal solutions, surface plasmon modes (SPMs), terahertz (THz) waveguides.

1. Introduction

The terahertz (THz) frequency region has attracted a huge amount of research effort in recent years and is emerging as a key technology for a number of applications. Considerable interest in THz devices has been created in the field of imaging [1], sensing [2], and scanning microscopy [3], [4]. The development of THz sources and receivers has also increased the demand for low-loss THz waveguides [5], which can be used as interconnects in integrated THz devices for higher speed and wideband communications. The lack of a compact and low-loss interconnect has limited the capacity for THz components to be placed either in close proximity to each other or else to use free space as the propagation medium, which then requires bulky components [6], [7]. A low-loss waveguide can be used to replace such bulky components with compact, integrated circuits.

The major hurdle for THz guiding is that most of the materials considered exhibit high absorption losses in this region of the spectrum [8]. Conventional dielectrics tend to be lossy at THz frequencies, whereas metals show low propagation loss owing to their high conductivities. To reduce absorption loss, waveguides can be designed such that less power stays within the lossy material and most of the power is guided through the air [9]. Amongst the techniques used so far, photonic crystal fiber [10], [11], porous fiber [12]–[14], hollow Bragg fiber [15], metal clad hollow core

[5], [16]–[18], and ferroelectric clad fiber [15], [19] can be mentioned, and all these approaches guide a significant portion of the power through air.

Among various approaches considered, a metal clad guide which supports surface plasmon modes (SPMs) is one of the most promising because of low loss in both active components and passive waveguides [5]. Surface plasmon polaritons (SPPs) are electromagnetic waves that propagate along the interface between a metal and a dielectric and decay evanescently on both sides of the interface. They are created because of the resonant interaction of the free electrons of the metal with the electromagnetic field of incident light wave [20]. Recently, it has been shown, both experimentally [18] and via numerical simulations [5], that a dielectric-coated metal-clad hollow core circular waveguide yields low loss at THz frequencies. Such flexible guides are more suitable to deliver high power electromagnetic waves to a target, instead of using free space transmission. Previously, Miyagi and Karasawa [21] suggested that a rectangular hollow core guide would be expected to have a lower bending loss, compared with a circular waveguide of a similar bore. A previous study by the authors [5] also shows that polarized modes in circular waveguides are not circular due to the boundary conditions at the metal–dielectric interface, even though the superposition of two degenerate polarized modes produces radially symmetric unpolarized modes. With these noncircular polarized modes being degenerate, the polarization state of the beam will not be stable. It is expected that modes in a rectangular waveguide can be designed not to be degenerate, and the polarization condition can be maintained in such a waveguide.

In this paper, the characterization and optimization of a dielectric-coated hollow core rectangular waveguide is presented. The goal was to find an optimized condition of the guide so that it supports low-loss propagation at THz frequencies and which will be small in size and easy to fabricate. Several surface plasmonic modes have been studied in the waveguide under two main conditions: with and without dielectric coating inside the metal cladding. To obtain strong field confinement and low-loss propagation at THz frequencies, several parameters of the structure were varied. The analysis carried out has revealed that introducing the dielectric coating minimizes the loss of the H_{12}^{x} mode of the guide significantly and transforms the mode shape into one that is Gaussian like, which should be easier to couple to transmitters and receivers. It has also been indicated that, by choosing appropriate parameters, the guide shows very low loss with a relatively small guide size.

2. Method of Analysis

A full-vectorial finite-element method (FEM) is used in this study to obtain the modal solutions of the hollow core rectangular waveguides. Since the early 1980s, this method has been adopted to analyze various low and high-frequency electromagnetic field problems and is widely used in the analysis of both microwave structures and optical guided-wave devices [22]. The vector FEM, which is based on the full-vectorial $\mathbf{H}$-field formulation, is considered to be one of the most accurate, numerically efficient, and versatile modal solution techniques. The full-vectorial formulation is based on the minimization of the following functional [22], in terms of the nodal values of the full $\mathbf{H}$-field vector:

$$\omega^2 = \frac{\int \left[(\nabla \times \mathbf{H})^* \cdot \epsilon^{-1} (\nabla \times \mathbf{H}) + p(\nabla \cdot \mathbf{H})^* (\nabla \cdot \mathbf{H}) \right] dx\, dy}{\int \mathbf{H}^* \cdot \mu \mathbf{H}\, dx\, dy} \tag{1}$$

where $\mathbf{H}$ is the full-vectorial magnetic field, * denotes a complex conjugate and its transpose, ω^2 is the eigenvalue (where ω is the angular frequency of the wave), ϵ and μ are the permittivity and permeability, respectively, and p is the dimensionless penalty parameter. The penalty function approach has been incorporated to impose the divergence-free conditions of the magnetic field to reduce the appearance of spurious modes [23]. The full-vectorial $\mathbf{H}$-field based finite-element modal solution is used to find the different optical modes of propagation, their propagation constants, loss values, and their corresponding full-vectorial field components.

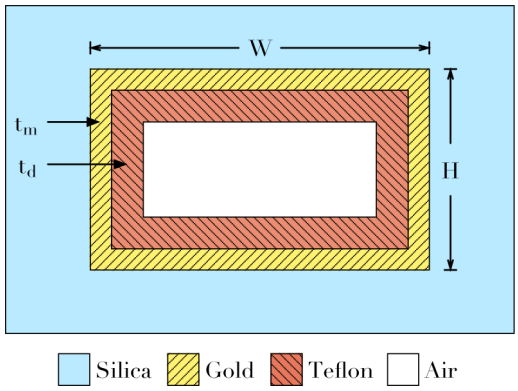

Fig. 1. Schematic diagram of the hollow core rectangular waveguide with a dielectric coating inside the air core, where W is the guide width, H is the height of the guide, t_m is the metal thickness, and t_d is the thickness of the dielectric coating.

3. Rectangular Hollow Core Guide

The structure considered here is composed of a thin metal clad silica waveguide with an air core. It was suggested previously [24] that by using a soldering technique to join two sets of parallel horizontal and vertical metal-clad dielectric slabs, such a waveguide can be fabricated readily. As the decay length at the gold–air interface will be much longer than that at the silica–gold interface, the electromagnetic field at the outer surface of the guide will decay more quickly. Hence, the host material, i.e., silica, in this case, has a negligible effect on the modes guided in the air core, and any other dielectric material can be used. At an operating frequency of 2.5 THz, the loss associated with the air is considered, and its complex refractive index was taken as $1.0 + j1.1 \times 10^{-6}$ [5]. Initially, the noble metal, i.e., gold (Au), having a refractive index $n_m = 281.55 + j419.74$ [25], has been considered as the cladding material. The width W and height H of the guide and the cladding thickness t_m were varied. To study the effect of the dielectric coating on the modal loss, a thin layer of Teflon deposited at the inner surface of the metal cladding was considered. A plasma vapor deposition process can be used to deposit Teflon on the metal during the fabrication process. Fig. 1 shows a schematic diagram of the rectangular cross section of the waveguide with a dielectric coating. A similar technique applied to a hollow core fiber has been studied [5] and fabricated [18] previously, where in that case, polystyrene was used as the dielectric coating material.

Quasi-TM modes with a dominant H^x field would form SPP modes at the horizontal metal–dielectric interface, whereas quasi-TE modes with the dominant H^y field can form SPP modes at the vertical metal/dielectric interface. In this paper, only the quasi-TM modes are reported; however the quasi-TE modes would show similar features. This structure supports the SPMs at two metal–dielectric interfaces: one at the outer silica–gold interface and the other at the gold–air interface inside. The decay length at the gold–air interface is much higher than that at the silica–gold interface. Again, in Insulator–Metal–Insulator (IMI) structures, the decay length of the odd-coupled mode is much higher than that of the even-coupled mode [26]. In this structure, at all four interfaces at the four sides, both sides of the metal cladding are surrounded by two different dielectrics. However, as the decay length at the gold–air interface will be much longer than that at the silica–gold interface, the electromagnetic field at the outer surface of the guide will decay faster. Since the refractive indices of the inner and outer claddings are different, their phase velocities are also different, and they do not couple effectively to form supermodes across the metal layer. On the other hand, the SPP modes at the upper and lower metal/air interfaces with longer decay lengths will couple to form supermodes as they are also phase matched. When these two modes couple in an even-like manner, an air-guided mode is formed.

It was observed that when the width and height of the waveguide were large compared with the wavelength, the waveguide supports many modes, and the real part of their effective indices (n_{eff}) are closer to the refractive index of the air core. In this paper, the fundamental H^x_{10} and four higher

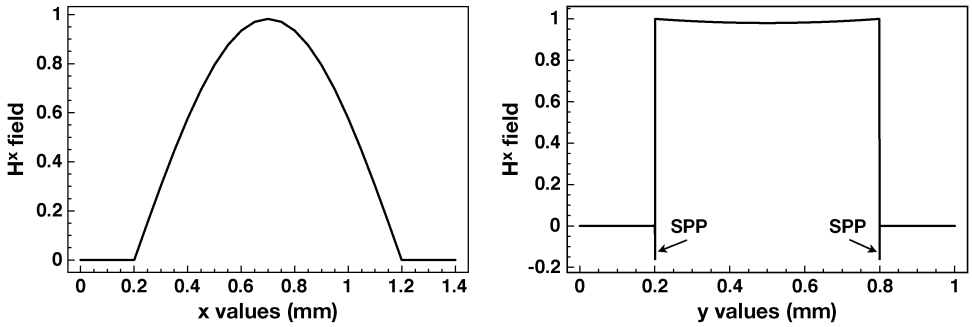

Fig. 2. H_{10}^x field profile along (a) the horizontal and (b) the vertical directions, respectively, in the hollow core rectangular waveguide with $W = 1.0$ mm, $H = 0.6$ mm, $t_m = 0.7$ μm, and $t_d = 0$.

order quasi-TM modes H_{20}^x, H_{30}^x, H_{11}^x, and H_{12}^x were studied. The contour profiles of these modes are shown later. Using a familiar nomenclature for the integrated optical waveguides, the waveguide modes were defined as H_{mn}^x, where H^x is the dominant $\mathbf{H}$-field component, and the subscripts m and n depict the field maxima along the x and y coordinates, respectively. The H^x field profile of the fundamental H_{10}^x mode along the horizontal and vertical directions are shown in Fig. 2(a) and (b), respectively. For this mode, identical SP modes existing at the top and bottom metal–dielectric interfaces couple together to form an even-like supermode along the vertical (y) direction, as presented in Fig. 2(b). Two plasmonic peaks at the gold–air interfaces are clearly visible and are shown by arrows in Fig. 2(b). However, the boundary condition along the vertical metal interfaces on the two side walls forces H^x to be zero there. Therefore, a half sine wave curve is formed along the horizontal direction, as can be seen in Fig. 2(a). On the other hand, the H_{11}^x mode is the result of the odd coupling between the SP modes of the top and bottom claddings. However, the H_{12}^x mode has a higher order variation along the y direction. Besides showing two sharp plasmonic peaks at the metal interfaces, this mode also shows two additional zero-crossings. The H_{20}^x and H_{30}^x modes follow a similar profile as the H_{10}^x along the y direction, but their profiles change along the horizontal (x) direction showing two and three field extrema, respectively. Before considering possible dielectric coatings inside the metal cladding, several parameters of the guide, namely the height, width, and the metal thickness, were varied to observe their effect on the modal properties, examining the effective index and the loss values for all of the five modes mentioned above. The effective index n_{eff} of a given mode is a normalized propagation parameter, which can be defined by $n_{eff} = (\beta/k_0) = n_{re} + jn_{im}$, where $\beta = \beta_{re} + \beta_{im}$ is the complex propagation constant of that mode, and k_0 is the free space wavenumber defined as $k_0 = \omega\sqrt{\mu\epsilon} = (2\pi/\lambda)$. The absorption coefficient is $\alpha_{WG} = 2\beta_{im}$ [27]. From this coefficient, the value of loss (in decibels per meter) was calculated as $loss = 8.6858896\beta_{im}$. This expression is used for all the calculations of loss throughout this paper.

3.1. Effect of Change in Guide Height

Fig. 3 shows the variations of the real part of effective index (n_{eff}) and the loss with the waveguide height H. The height of the guide was varied from 0.4 mm to 1.0 mm while keeping the width and cladding thickness constant at 1.0 mm and 0.7 μm, respectively. It can be seen from Fig. 3(a) that for the H_{10}^x, H_{20}^x, and H_{30}^x modes, n_{eff}'s do not change much with the height. When the height is gradually reduced from 1.0 mm to 0.4 mm at an interval of 0.1 mm, the deviation in effective index (from that of height 1.0 mm) is only about 0.0073%, 0.0075%, and 0.0076% for the H_{10}^x, H_{20}^x, and H_{30}^x modes, respectively. This is because, although these three modes have different variations along the x direction, their field profiles along the y direction are constant, and these are not affected by the changing height. Due to the much larger decay length in air, compared with the change of height of the guide, these modes do not show significant variation of their effective index

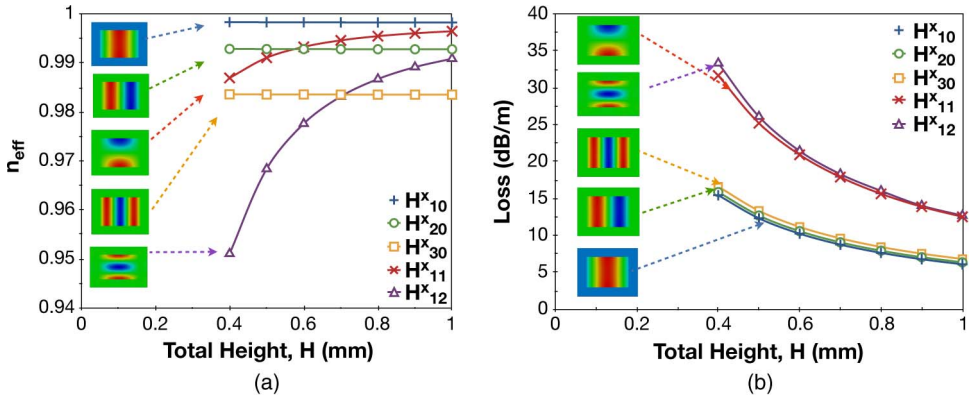

Fig. 3. (a) Real part of effective index. (b) Loss of all the five modes as a function of height at $W = 1.0$ mm, $t_m = 0.7$ μm, and $t_d = 0$.

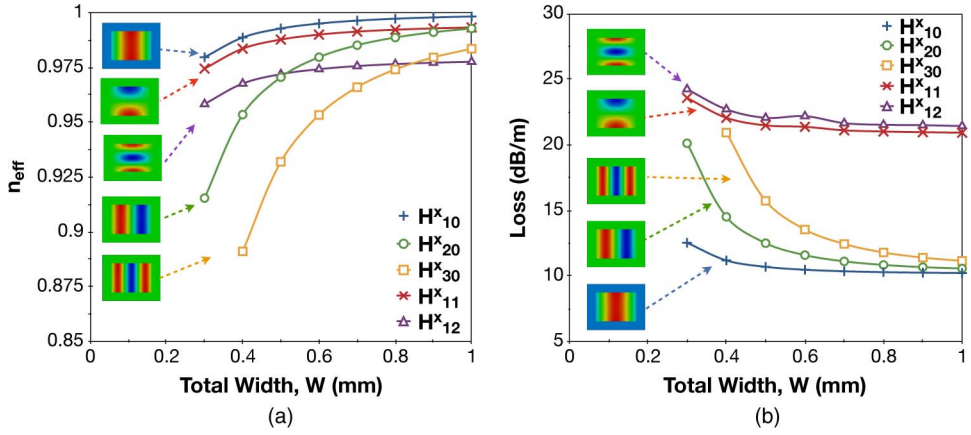

Fig. 4. (a) n_{eff}. (b) Loss of all the five modes as a function of guide width at $H = 0.6$ mm, $t_m = 0.7$ μm, and $t_d = 0$.

values. However, the higher order modes have slightly smaller effective indices than those of lower order. On the other hand, the effective index curves of the H^x_{11} and H^x_{12} modes fall more rapidly as the guide height is decreased, showing a stronger dependence on the waveguide height H as their spatial variation is changed with the height. The H^x_{12} mode has a sharp decaying curve of its effective index when the waveguide height is reduced.

Fig. 3(b) shows the variation of the modal loss with height for all the five modes. It can be observed that the modal losses of the guide increase exponentially with the reduction of height for all the modes. The loss values, for the H^x_{10}, H^x_{20}, and H^x_{30} modes, are very close to each other, and their rate of change is almost identical. For these three modes, it can be noted that all the loss values are very similar when the waveguide height H is large, but the higher order modes have slightly higher losses than those of lower order. However, losses increase at a much higher rate in the case of the H^x_{11} and H^x_{12} modes where the field depends strongly on the height H. These values are also much greater compared with the other three modes. The H^x_{10} mode has the lowest loss value among all the modes shown here. The H^x field profiles for all the five modes are shown as insets in Fig. 3(a) and (b).

3.2. Effect of Change in Guide Width

In order to observe the dependence of the effective index and the loss values on the width of the rectangular guide, this parameter (denoted by W) was varied from 0.5 mm to 1.0 mm for all the

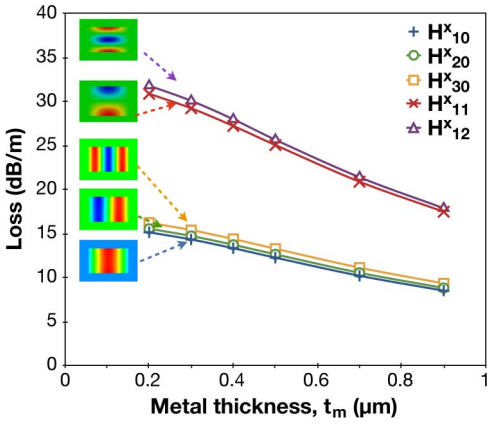

Fig. 5. Loss of all the five modes as a function of metal thickness t_m at $W = 1.0$ mm, $H = 0.6$ mm, and $t_d = 0$.

five modes. Fig. 4(a) depicts the variation of n_{eff} for the five modes with respect to width for a constant height $H = 0.6$ mm and a metal thickness $t_m = 0.7$ μm. The curves suggest that the values of n_{eff} decrease for all the modes, with decreasing width. For the H^x_{10}, H^x_{11}, and H^x_{12} modes, the rate of decrement of the n_{eff}'s are similar due to the fact that, in the horizontal direction, the variation of their modal field profiles are similar. However, the lower order modes exhibit larger effective indices. On the other hand, for the H^x_{20}, and H^x_{30} modes, their n_{eff} values reduce much more rapidly because of the faster change in the mode profiles in the horizontal direction with the width variation. The rate of decrement is much greater for the higher order mode than for its lower order counterpart.

The propagation loss for the H^x_{10}, H^x_{11}, and H^x_{12} modes have similar incremental rates with decreasing width, as can be seen from Fig. 4(b). The loss values for these modes do not increase significantly as the losses arise predominantly due to the metal confinement in the top and the bottom dielectric–metal interfaces. The boundary conditions at the left and right interfaces demand a zero H^x field which does not interact with the mode profile. On the other hand, for the H^x_{20} and H^x_{30} modes, the losses increase sharply while the width is decreased. This arises because the change of the mode profile in the horizontal direction also affects the interaction at the upper and lower metal–dielectric interfaces.

3.3. Effect of Change in Metal Thickness

Next, the effect of the metal thickness on the modal loss was also studied. When the thickness of the Au cladding layer was varied over a range 0.2 μm $< t_m <$ 0.9 μm, the loss curves for all the five modes showed a similar nature as given in Fig. 5. In this case, the width and the height of the guide were taken as 1.0 mm and 0.6 mm, respectively. The propagation loss values follow a decreasing trend with increasing metal thickness. However, the higher order modes show higher values of loss than those of the lower order, particularly the higher order modes in the vertical direction. The effective indices of the modes do not change significantly with the cladding thickness, and these are not shown here.

4. Dielectric-Coated Design

4.1. Choice of Dielectric

In the work previously reported by Themistos *et al.* [5], polystyrene was used as the dielectric material for the coating inside the metal cladding and the complex refractive index for this material was reported to be $1.58 + j0.0036$ at 2.5 THz. Operating at the same operating frequency, it has been observed that Teflon is a lower loss medium with a complex refractive index

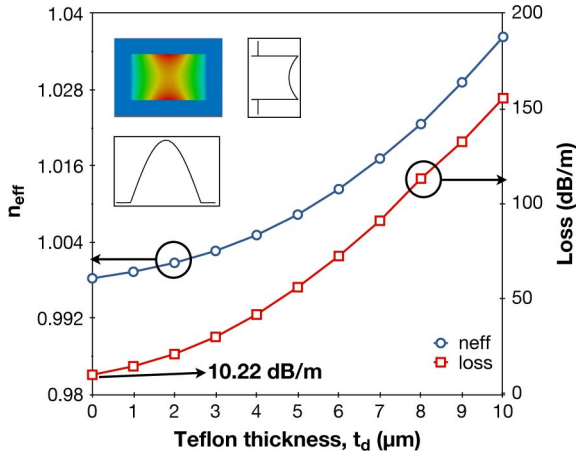

Fig. 6. n_{eff} and loss of the H_{10}^x mode as a function of Teflon thickness at $W = 1.0$ mm, $H = 0.6$ mm, and $t_m = 0.7$ μm.

$n_d = 1.445 + j0.00119$ [28], [29]. For this reason, the effect of a layer of Teflon deposited inside the metal cladding in this structure was studied. A guide width of 1.0 mm, a height of 0.6 mm, and a metal thickness of 0.7 μm were considered for incorporation in the simulation, although these parameters can also be optimized as necessary. The effect of the Teflon thickness on the different modes was observed, which is presented in the following sections.

4.2. Effect of Teflon Thickness

Initially, the effect of the Teflon thickness on the fundamental H_{10}^x mode, which also shows minimum loss values, was investigated. This feature is of particular interest where low-loss applications are concerned. After considering a coating of Teflon, this mode was analyzed to find a possible low-loss condition. It was observed that in the absence of the Teflon coating, the H^x field exhibits a sharp rise at the air–Au interfaces at the top and the bottom but maintains a fairly constant profile at the central air core, details of which are presented in Fig. 2(b). As the Teflon coating was introduced inside the metal, the field profile deteriorates with a dip at the center of the waveguide. Increasing the thickness of the Teflon layer results in a decoupling of the two SPMs of the top and bottom interfaces as a significant part of the field penetrates into the Teflon layer and interacts with the metal cladding when the Teflon coating is applied. Hence, the field inside the air core decreases with the increase in the Teflon thickness. As a result, the propagation loss also increases. Fig. 6 presents the variation of the effective index and the loss curves of the H_{10}^x mode with the change in the Teflon thickness. This figure shows that the effective index of the mode rises exponentially with an increase in the Teflon thickness because power is more confined in the high index Teflon layer. The loss curve for the mode shows similar characteristics, as increasing the Teflon layer suggests that the field confinement at the metal–Teflon interface increases, which gives rise to the loss value seen. The top left inset in the figure shows the contour field profile of this mode at a Teflon thickness of $t_d = 1$ μm, whereas the other two insets present the H^x field profiles of the same mode along the horizontal and vertical directions passing through the center of the guide. It can be noted that the minimum loss achievable with this mode is 10.22 dB/m when no Teflon coating was applied.

It has already been mentioned that the field profile at the center of the waveguide reduces when the thickness of the Teflon layer was increased and this is shown in Fig. 7(a), where the normalized H^x field amplitude at the center of the waveguide (normalized to its maximum value) is plotted against the Teflon thickness. It can be noted that when the Teflon thickness is 7 μm, the field value at the center of the waveguide is only 10% of the maximum field at the edges.

The propagation loss depends on the power confinement in the different layers and their corresponding loss tangent values. The power confinement in any particular layer (constituting the

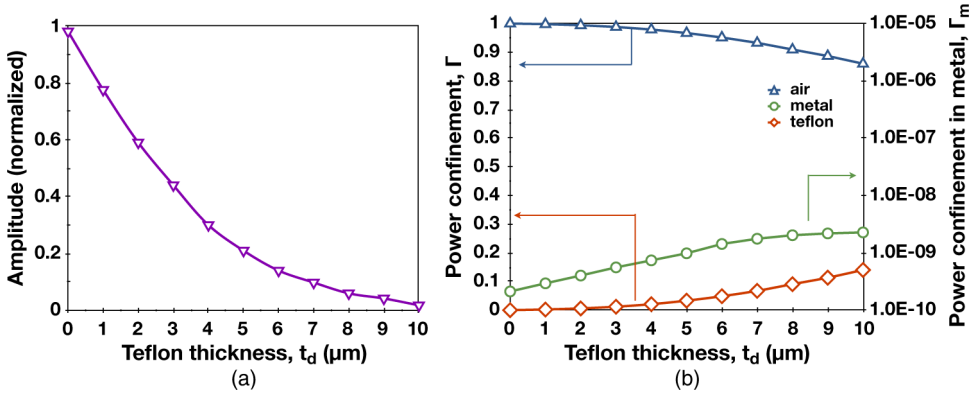

Fig. 7. (a) Normalized amplitude of the mode profile taken at the center of the profile in the vertical direction and (b) power confinement factors in air, in Teflon (Γ_d), and in metal (Γ_m) as a function of Teflon thickness for the H^x_{10} mode when $W = 1.0$ mm, $H = 0.6$ mm, and $t_m = 0.7$ μm.

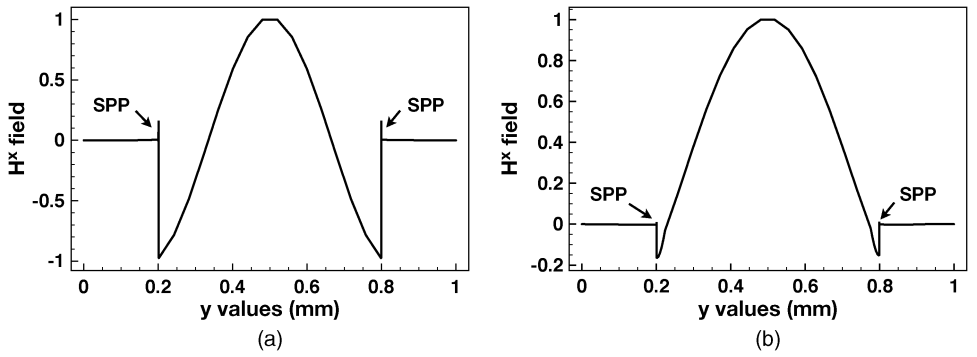

Fig. 8. Normalized H^x field profiles of the H^x_{12} mode along the vertical direction for two different Teflon thicknesses (a) at $t_d = 0$ μm and (b) at $t_d = 21$ μm when $W = 1.0$ mm, $H = 0.6$ mm, and $t_m = 0.7$ μm.

guide) is calculated by normalizing the power in that layer to the total power. The fraction of the power confined in the air core, the Teflon, and the metal cladding for the H^x_{10} mode are shown in Fig. 7(b) for different Teflon thicknesses. This figure clearly illustrates the fact that as the thickness of the Teflon layer is increased, the power confinement in the Teflon increases (left hand scale) as more field is drawn into that layer. This also reduces the amount of power confined in the air core (left hand scale). The power confinement in the Au layer is also higher for a thicker Teflon layer, which strongly contributes to the modal loss values. It should be noted that the power confinement in the metal is shown with reference to the right hand scale in Fig. 7(b). Although this fractional value is smaller, the dominant loss value contribution comes from the power confinement in this layer.

The other higher order modes H^x_{20}, H^x_{30}, and H^x_{11} have also been studied. They show similar characteristics to the H^x_{10} mode, with both n_{eff} and the loss increasing exponentially with increasing Teflon thickness, but these are not shown here. However, the H^x_{12} mode shows interesting modal properties after the Teflon coating is added, and this is shown and discussed in the remainder of the paper.

It has been noticed that the presence of the Teflon layer strongly affects the field profile of the H^x_{12} mode. The field profiles for the H^x_{12} mode for different Teflon thicknesses have also been investigated. These field profiles for the H^x_{12} mode along the y direction for Teflon thicknesses of 0 μm and 21.0 μm are shown in Fig. 8(a) and (b), respectively. For both these cases, the H^x field profiles show a rapid change at the metal–Teflon interface (shown by arrows), exhibiting a

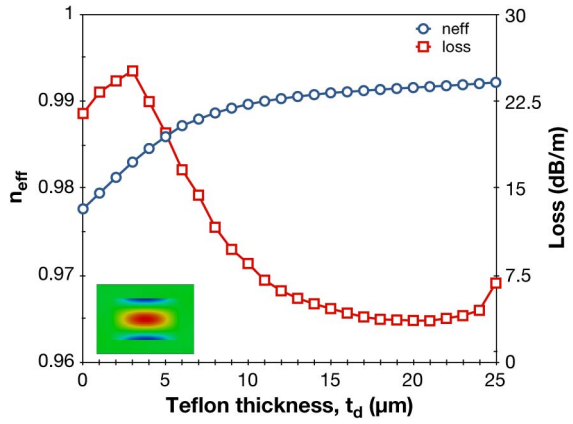

Fig. 9. n_{eff} and loss of the H_{12}^x mode as a function of Teflon thickness at $W = 1.0$ mm, $H = 0.6$ mm, and $t_m = 0.7$ μm.

plasmonic nature. This mode also shows large negative fields at the Au–Teflon interfaces, in a similar way to the case when the Teflon was absent (as mentioned above in Section 3). However, for a smaller thicknesses of the Teflon layer, the field profile has significant sidelobes of negative polarity, and they interact mainly with the metal cladding, but when the Teflon thickness increases, a significant part of the field moves into the central air core, with the sidelobes reducing in amplitude. This situation is shown in the field profile for a Teflon thickness of 21.0 μm in Fig. 8(b). As can be seen, it has an almost Gaussian shaped profile at the central air core region for a thick Teflon layer. Therefore, applying a Teflon coating can minimize the two negative lobes, and this mode can be more suitable for launching through a waveguide from a Gaussian shaped source. The smaller sidelobes also generate plasmonic peaks of smaller values [shown by arrows in Fig. 8(b)], and in turn, these lower the loss inside the metal layers.

The variation of the effective index and the loss characteristics with the change of the Teflon thickness for the H_{12}^x mode have been investigated and are presented together in Fig. 9. As with the H_{10}^x mode, the loss value for the H_{12}^x mode started to rise initially, but then, it reduces after a Teflon thickness of 3.0 μm is reached. As mentioned above, for this mode, the two minor lobes of opposite polarity contain a significant amount of power. When these two lobes interact with the metal cladding, the loss in the metal layer starts to fall because a higher level of the field is shifted from the metal to the lower loss Teflon layer. Hence, the loss of this mode is much higher than that of the H_{10}^x mode for lower values of the Teflon thickness. The total loss is mainly governed by the attenuation in the metal for a lower Teflon thickness. However, as the Teflon thickness increases to a value above 3.0 μm, the Teflon layer starts interacting with the metal cladding, the sidelobes of the modal field profile start to reduce in amplitude, and more field is trapped inside the air core. The central Gaussian lobe becomes predominant. The lower confinements in the metal and the Teflon layers result in a reduction of the total loss. The loss characteristics of the waveguide, along with the individual contributions of the metal and the Teflon layers, are shown in Fig. 10 with the variation of the Teflon thickness. The loss in the Teflon layer is shown by square symbols, whereas circular symbols are used to denote the loss in the metal layer in Fig. 10.

When the Teflon thickness is further increased, the loss in the Teflon layer reaches the same order of magnitude of the metal losses and crosses it (the metal loss) at a Teflon thickness of $t_d = 16$ μm. At a Teflon layer thickness of 21.0 μm, the minimum loss is achieved. Beyond this thickness, the loss in the Teflon starts to increase. The high refractive index of Teflon compared with that of air draws away power from the central Gaussian lobe and the confinement in Teflon becomes predominant, compared with that in metal. Thus, the total loss increases again. The lowest loss found for this configuration is 3.55 dB/m, which is obtained at a Teflon layer thickness of 21.0 μm. This is only one third of the lowest loss of the H_{10}^x mode, as well as a significantly low value of loss compared with previously reported THz waveguides. McGowan *et al.* [30] reported a

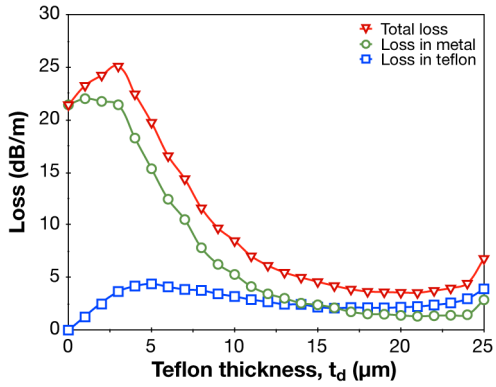

Fig. 10. Variation of the total Loss and loss in metal and in Teflon for the H_{12}^x mode as a function of Teflon thickness for $W = 1.0$ mm, $H = 0.6$ mm, and $t_m = 0.7$ μm.

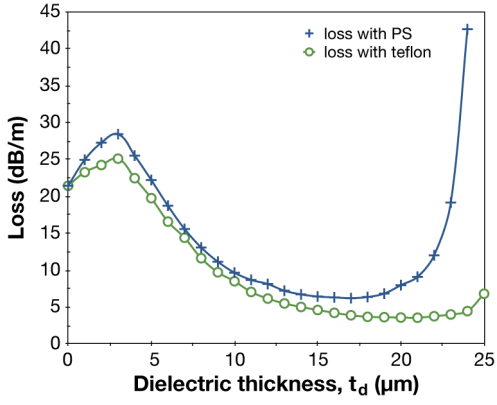

Fig. 11. Comparison of loss characteristics of the H_{12}^x mode for two dielectric coatings (Polystyrene and Teflon) as a function of the dielectric thickness t_d at a metal thickness $t_m = 0.7$ μm when $W = 1.0$ mm and $H = 0.6$ mm.

loss of about 300 dB/m, Hidaka *et al.* a loss of 6.5 dB/m [19], and Harrington *et al.* reported a loss of 3.9 dB/m [17] at THz frequency. The power confinement in the central air core was determined to be around 0.99 throughout the whole range of Teflon thickness studied.

4.3. Polystyrene Versus Teflon

A similar study was also performed with Polystyrene, and the loss comparison between the Polystyrene and the Teflon is presented in Fig. 11. Both show a similar trend, revealing a minimum loss at $t_d = 21$ μm and $t_d = 17$ μm, with minimum loss values of 3.55 dB/m and 6.2 dB/m for Teflon and Polystyrene, respectively. It clearly shows that the minimum loss for the H_{12}^x mode with Polystyrene is significantly higher than for a similar guide with Teflon coating, as was predicted earlier in Section 3.1. This is due to the higher loss tangent of Polystyrene than that of Teflon.

4.4. Effect of Changing Metal

A further study of the H_{12}^x mode was performed for two other metal claddings, i.e., Ag and Cu, having effective indices of $308 + j532$ and $250.52 + j345.42$, respectively, at 2.5 THz. Fig. 12(a) shows the comparison of the losses for different Teflon thicknesses at a constant metal thickness $t_m = 0.7$ μm for the three metals: Au, Ag, and Cu. It can be seen that the minimum values of loss with the variation of the Teflon thickness is 3.55 dB/m, 2.94 dB/m, and 4.21 dB/m for Au, Ag, and

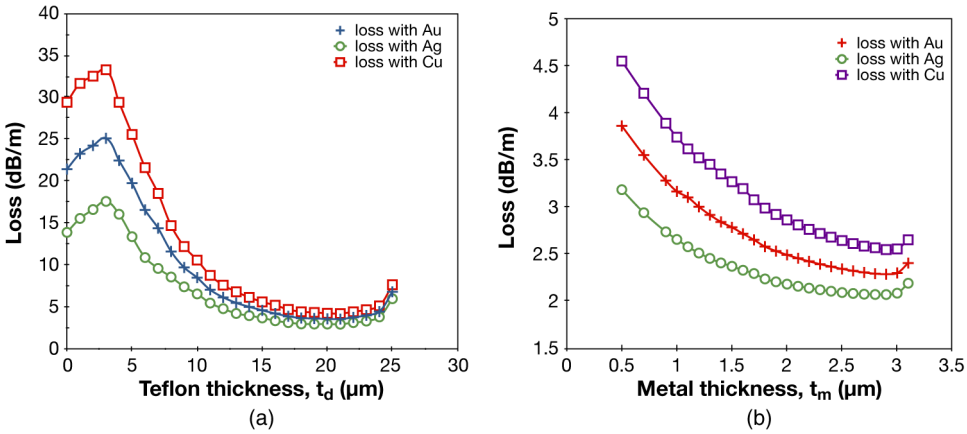

Fig. 12. Loss of the H_{12}^x mode as a function of (a) Teflon thickness t_d at a metal thickness $t_m = 0.7$ μm. (b) Metal thickness t_m when the Teflon thickness $t_d = 18$ μm, $W = 1.0$ mm, and $H = 0.6$ mm.

Cu, respectively, at the same Teflon thickness value $t_d = 21$ μm. A pure metal with a pure imaginary refractive index does not contribute to the modal loss. On the other hand, for a lossy metal, its imaginary part (n_i) is bigger than its real part (n_r), and the real part contributes to the loss. Of the three metals mentioned above, silver (Ag) has the lowest n_r/n_i ratio, at 2.5 THz, and hence, it suffers the lowest loss, as can be seen from the results obtained.

4.5. Effect of Metal Thickness

Further analysis on the effect of the cladding (metal) thickness on the characteristics of the guide for the three metals mentioned above was performed. It has been observed that changing the metal thickness has also gradually shifted the minimum loss of the guide from a Teflon thickness of 21 μm to 18 μm. Fig. 12(b) shows the loss characteristics of the guide with different metal thicknesses (with the Teflon thickness taken as 18 μm) for three different metal claddings. As can be seen from this figure, as the metal thickness increases, the loss of the guide further decreases to a metal thickness value of 2.9 μm. Beyond a metal thickness of 2.9 μm, the loss of the guide starts to increase again. For a Teflon thickness $t_d = 18$ μm, the minimum loss was found with an Ag-coated guide with a value of 2.07 dB/m, whereas using Cu and Au, the losses are 2.54 dB/m and 2.286 dB/m, respectively. This clearly shows that the loss value can be minimized by adjusting various parameters of the waveguide.

5. Conclusion

In recent years, the unique properties and promising applications of THz waves have led to a series of significant advances within the THz frequency range, providing new opportunities. A low-loss THz interconnect will soon be required, arising from the demand for high-speed devices and wideband communications. A rigorous finite-element approach based on a full-vectorial $\mathbf{H}$-field formulation has been used to study the characteristics of a hollow core Teflon-coated rectangular plasmonic waveguide at THz wavelengths. The goal of the work was to find the mode with the minimum loss and the optimal configuration of the waveguide for that mode. Detailed studies have been performed by varying the height and width of the waveguide, the Teflon coating thickness, and the metal cladding thickness to optimize the waveguide. The loss can be minimized by selecting a suitable low-loss dielectric coating, a metal, and its thickness for a given dimension of the THz waveguide. After the design optimization, the H_{12}^x mode was found to have the lowest loss among all the modes considered here. Moreover, in the optimum configuration, this mode resembles a near-Gaussian shape in both the transverse directions, and using this would facilitate better coupling to the input and output sections. Different metals were also used to design the guide and determine the minimum loss conditions. A study using Polystyrene as the coating

dielectric was also performed to compare the loss characteristics with those of Teflon. As the dimensions of the layers varied considerably from the millimeter to submicrometer, this FEM based approach was used to exploit the irregular size elements and, thus, to provide the flexibility of accurate modeling.

In the end, the lowest loss was found with an Ag cladding and a Teflon coating. It was shown here that 18.0 μm thickness (which is the optimized value of the dielectric coating with a Ag cladding thickness of 2.9 μm) produces the minimum loss within the scope of this study. With the optimal configuration, the loss of the waveguide reported here for $W = 1.0$ mm and $H = 0.6$ mm is 2.07 dB/m. The loss can be further reduced by considering a larger waveguide, which compares much favorably with the previously studied [5] circular Polystyrene-coated guide exhibiting a 2.1-dB/m loss for a 2-mm diameter bore. However, by increasing the waveguide height and the width, the loss can be further reduced. Due to the rectangular shape of the guide, the horizontally and vertically polarized modes will not be degenerate. Hence, such a low-loss rectangular waveguide, which can be made flexible, would be able to maintain the polarization state of the input wave and may be easier to integrate with other components than would a circular structure.

References

[1] Q. Chen, Z. Jiang, G. Xu, and X. Zhang, "Near-field terahertz imaging with a dynamic aperture," *Opt. Lett.*, vol. 25, no. 15, pp. 1122–1124, Aug. 2000.

[2] R. Jacobsen, D. Mittleman, and M. Nuss, "Chemical recognition of gases and gas mixtures with terahertz waves," *Opt. Lett.*, vol. 21, no. 24, pp. 2011–2013, Dec. 1996.

[3] J. Zhang and D. Grischkowsky, "Waveguide terahertz time-domain spectroscopy of nanometer water layers," *Opt. Lett.*, vol. 29, no. 14, pp. 1617–1619, Jul. 2004.

[4] G. Gallot, S. Jamison, R. McGowan, and D. Grischkowsky, "Terahertz waveguides," *J. Opt. Soc. Amer. B*, vol. 17, no. 5, pp. 851–863, 2000.

[5] C. Themistos, B. M. A. Rahman, M. Rajarajan, K. T. V. Grattan, B. Bowden, and J. Harrington, "Characterization of Silver/Polystyrene (PS)-coated hollow glass waveguides at THz frequency," *J. Lightw. Technol.*, vol. 25, no. 9, pp. 2456–2462, Sep. 2007.

[6] P. Siegel, "Terahertz technology," *IEEE Trans. Microw. Theory Tech.*, vol. 50, no. 3, pp. 910–928, Mar. 2002.

[7] C. Yeh, F. Shimabukuro, and P. Siegel, "Low-loss terahertz ribbon waveguides," *Appl. Opt.*, vol. 44, no. 28, pp. 5937–5946, Oct. 2005.

[8] B. Ung, A. Dupuis, K. Stoeffler, C. Dubois, and M. Skorobogatiy, "High-refractive-index composite materials for terahertz waveguides: Trade-off between index contrast and absorption loss," *J. Opt. Soc. Amer. B*, vol. 28, no. 4, pp. 917–921, Apr. 2011.

[9] C. Lai, B. You, J. Lu, T. Liu, J. Peng, C. Sun, and H. Chang, "Modal characteristics of antiresonant reflecting pipe waveguides for terahertz waveguiding," *Opt. Exp.*, vol. 18, no. 1, pp. 309–322, Jan. 2010.

[10] K. Nielsen, H. Rasmussen, A. Adam, P. Planken, O. Bang, and P. Jepsen, "Bendable, low-loss topas fibers for the terahertz frequency range," *Opt. Exp.*, vol. 17, no. 10, pp. 8592–8601, May 2009.

[11] H. Han, H. Park, M. Cho, and J. Kim, "Terahertz pulse propagation in a plastic photonic crystal fiber," *Appl. Phys. Lett.*, vol. 80, no. 15, pp. 2634–2636, Apr. 2002.

[12] A. Dupuis, A. Mazhorova, F. Désévédavy, M. Rozé, and M. Skorobogatiy, "Spectral characterization of porous dielectric subwavelength THz fibers fabricated using a microstructured molding technique," *Opt. Exp.*, vol. 18, no. 13, pp. 13 813–13 828, Jun. 2010.

[13] A. Dupuis, J. Allard, D. Morris, K. Stoeffler, C. Dubois, and M. Skorobogatiy, "Fabrication and THz loss measurements of porous subwavelength fibers using a directional coupler method," *Opt. Exp.*, vol. 17, no. 10, pp. 8012–8028, May 2009.

[14] A. Hassani, A. Dupuis, and M. Skorobogatiy, "Low loss porous terahertz fibers containing multiple subwavelength holes," *Appl. Phys. Lett.*, vol. 92, no. 7, pp. 071101-1–071101-3, Feb. 2008.

[15] M. Skorobogatiy and A. Dupuis, "Ferroelectric all-polymer hollow Bragg fibers for terahertz guidance," *Appl. Phys. Lett.*, vol. 90, no. 11, pp. 113514-1–113514-3, Mar. 2007.

[16] T. Ito, Y. Matsuura, M. Miyagi, H. Minamide, and H. Ito, "Flexible terahertz fiber optics with low bend-induced losses," *J. Opt. Soc. Amer. B*, vol. 24, no. 5, pp. 1230–1235, May 2007.

[17] J. Harrington, R. George, P. Pedersen, and E. Mueller, "Hollow polycarbonate waveguides with inner Cu coatings for delivery of terahertz radiation," *Opt. Exp.*, vol. 12, no. 21, pp. 5263–5268, Oct. 2004.

[18] B. Bowden, J. Harrington, and O. Mitrofanov, "Silver/polystyrene-coated hollow glass waveguides for the transmission of terahertz radiation," *Opt. Lett.*, vol. 32, no. 20, pp. 2945–2947, Oct. 2007.

[19] T. Hidaka, H. Minamide, H. Ito, J. Nishizawa, K. Tamura, and S. Ichikawa, "Ferroelectric PVDF cladding terahertz waveguide," *J. Lightw. Technol.*, vol. 23, no. 8, pp. 2469–2473, Aug. 2005.

[20] H. Raether, *Surface Plasmons*. New York: Springer-Verlag, 1988.

[21] M. Miyagi and S. Karasawa, "A comparative study of rectangular and circular dielectric-coated metallic waveguides for CO_2 laser light: Theory," *Opt. Commun.*, vol. 68, no. 1, pp. 18–20, Sep. 1988.

[22] B. M. A. Rahman and J. B. Davies, "Finite-element solution of integrated optical waveguides," *IEEE/OSA J. Lightw. Technol.*, vol. LT-2, no. 5, pp. 682–688, Oct. 1984.
[23] B. M. A. Rahman and J. B. Davies, "Penalty function improvement of waveguide solution by finite elements," *IEEE Trans. Microw. Theory Tech.*, vol. MTT-32, no. 8, pp. 922–928, Aug. 1984.
[24] H. Machida, Y. Matsuura, H. Ishikawa, and M. Miyagi, "Transmission properties of rectangular hollow waveguides for CO_2 laser light," *Appl. Opt.*, vol. 31, no. 36, pp. 7617–7622, Dec. 1992.
[25] M. Ordal, L. Long, R. Bell, S. Bell, R. Bell, R. Alexander, and C. Ward, "Optical properties of the metals Al, Co, Cu, Au, Fe, Pb, Ni, Pd, Pt, Ag, Ti, and W in the infrared and far infrared," *Appl. Opt.*, vol. 22, no. 7, pp. 1099–1120, Apr. 1983.
[26] P. Berini, "Plasmon-polariton waves guided by thin lossy metal films of finite width: Bound modes of asymmetric structures," *Phys. Rev. Ser. B*, vol. 63, no. 12, p. 125 417, Mar. 2001.
[27] K. H. Schlereth and M. Tacke, "The complex propagation constant of multilayer waveguides: An algorithm for a personal computer," *IEEE J. Quantum Electron.*, vol. 26, no. 4, pp. 627–630, Apr. 1990.
[28] Y. Jin, G. Kim, and S. Jeon, "Terahertz dielectric properties of polymers," *J. Korean Phys. Soc.*, vol. 49, no. 2, pp. 513–517, Aug. 2006.
[29] C. Winnewisser, F. Lewen, and H. Helm, "Transmission characteristics of dichroic filters measured by THz time-domain spectroscopy," *Appl. Phys. A, Mater. Sci. Process.*, vol. 66, no. 6, pp. 593–598, 1998.
[30] R. McGowan, G. Gallot, and D. Grischkowsky, "Propagation of ultrawideband short pulses of terahertz radiation through submillimeter-diameter circular waveguides," *Opt. Lett.*, vol. 24, no. 20, pp. 1431–1433, Oct. 1999.